Current Optics and Photonics
Vol. 3, No. 2, April 2019, pp. 143-149

ISSN: 2508-7266(Print) / ISSN: 2508-7274(Online)
DOI: https://doi.org/10.3807/COPP.2019.3.2.143

Shape Ellipticity Dependence of Exciton Fine Levels and Optical Nonlinearities in CdSe and CdTe Nanocrystal Quantum Dots

Hanyi Yang[1] and Kwangseuk Kyhm[1,2]*

[1]*Department of Physics Education, Pusan National University, Busan 46241, Korea*
[2]*Department of Optomechatronics, Pusan National University, Busan 46241, Korea*

(Received December 20, 2018 : revised February 4, 2019 : accepted February 12, 2019)

Shape ellipticity dependence of the exciton fine energy levels in CdTe and CdSe nanocrystal quantum dots were compared theoretically by considering the crystal structure and the Coulomb interaction of an electron and a hole. While quantum dot ellipticity changes from an oblate to prolate quantum dot via spherical shape, both the fine energy levels and the dipole moment in wurtzite structure of a CdSe quantum dot change linearly for ellipticity. In contrast, CdTe quantum dots were found to show a level crossing between the bright and dark exciton states with a significant change of the dipole moment due to the cubic structure. Shape ellipticity dependence of the optical nonlinearities in CdTe and CdSe nanocrystal quantum dots was also calculated by using semiconductor Bloch equations. For a spherical shape quantum dot, only 1^{L} dominates the optical nonlinearities in a CdSe quantum dot, but both 1^{U} and 0^{U} contribute in a CdTe quantum dot. As excitation pulse area becomes strong ($\sim\pi$), the optical nonlinearities of both CdSe and CdTe quantum dots are mainly governed by absorption saturation. However, in the case of a prolate CdTe quantum dot, the real part of the nonlinear refractive index becomes relatively significant.

Keywords : Quantum dots, Excitons, Shape ellipticity, Nonlinearity refractive index
OCIS codes : (160.4236) Nanomaterials; (260.7120) Ultrafast phenomena; (300.6240) Spectroscopy, coherent transient

I. INTRODUCTION

Currently, quantum dots are of great interest for both fundamental research and industrial applications due to their strong three dimensional quantum confinement effects [1]. For instance, a two-level system of the confinement states can be used as a qubit, and tunable fluorescence of nanocrystal quantum dots (NQDs) are used for bio-probe and display devices by controlling the size [2, 3]. Although the confinement energy levels of NQDs can be observed by absorption and photoluminescence (PL) spectrum [4-6], the presence of fine (~10 meV) energy levels were proposed theoretically. It was known that the fine energy levels of NQDs depend on not only the radius but also the shape ellipticity and the crystal structures of NQDs [7, 8], whereby the shape dependence of oscillator strength can also be obtained [9-11]. In order to observe the fine energy levels, high spectral-resolution photo-excitation luminescence (PLE) can be used for the ensemble NQDs. However, regarding randomly oriented NQDs dispersed on a substrate, micro-PL of a single NQD is necessary for accurate comparison with theory. Although much research has been reported on single NQD micro-PL, the fine energy levels have rarely been considered.

Additionally, optical nonlinearity of quantum dots can be applicable to various photonics technology such as nonlinear optical imaging and optical bio-sensors. While multi-photon processes of NQDs are often investigated, exciton optical nonlinearities were rarely reported. In this case, the shape ellipticity and fine energy levels should be considered. However, the shape dependence of optical nonlinearities of NQDs has never yet been reported. In this work, we have calculated theoretically the fine energy levels and dipole

*Corresponding author: kskyhm@pusan.ac.kr, ORCID 0000-0003-3646-3560
Color versions of one or more of the figures in this paper are available online.

This is an Open Access article distributed under the terms of the Creative Commons Attribution Non-Commercial License (http://creativecommons.org/licenses/by-nc/4.0/) which permits unrestricted non-commercial use, distribution, and reproduction in any medium, provided the original work is properly cited.

Copyright © 2019 Current Optics and Photonics

moments of CdSe and CdTe by considering the shape ellipticity and the crystal structure, and the nonlinear refractive index of each fine level was obtained by using the semiconductor Bloch equations.

II. THEORY

Suppose a spherical quantum dot (QD) with a radius a is surrounded by an infinite potential barrier, the ground state energy of an electron and a hole in the conduction and the fourfold degenerate valence band are given by $E_a = \frac{\hbar^2\pi^2}{2m_e^* a^2}$ and $E_h = \frac{\hbar^2 k^2(\beta)}{2m_{hh}^* a^2}$ respectively, where $\beta = m_{lh}^*/m_{hh}^*$ is the ratio of the light to heavy hole effective mass, and $k(\beta)$ is the first root of the equation $j_0(k)j_2(\sqrt{\beta}k) + j_2(k)j_0(\sqrt{\beta}k) = 0$. Thus, the exciton state of a spherical quantum dot is eightfold degenerate by two electron spin states ($1S_{3/2}^e$) and four hole spin states ($1S_{3/2}^h$). However, the eightfold degeneracy of the spherical band-edge exciton is split into spin-degenerate five levels (0^U, 0^L, $\pm1^U$, $\pm1^L$ and ±2) as a consequence of crystal structure, shape ellipticity, and electron-hole exchange interaction.

In the case of CdSe, the spin-orbit coupling should be considered due to the wurtzite structure, where the heavy-hole ($j = \frac{3}{2}$, $m_j = \pm\frac{3}{2}$) and light-hole ($j = \frac{3}{2}$, $m_j = \pm\frac{1}{2}$) bands become separate with an energy of crystal field ($\triangle_{cr}$). However, the diamond-like structure gives $\triangle_{cr} = 0$ in CdTe [12, 13]. Additionally, the non-sphericity energy ($\triangle_{sh}$) is associated with degree of ellipticity (μ) and $\triangle_{cr}$ as

$$\triangle_{sh} = \triangle_{cr} v(\beta) + 2\mu E_h(a,\beta)u(\beta), \tag{1}$$

$$v(\beta) = \int dr r^2 \left[R_0^2(a,r) - \frac{3}{5} R_2^2(a,r) \right], \tag{2}$$

$$\int dr r^2 \left[R_0^2(a,r) + R_2^2(a,r) \right] = 1, \tag{3}$$

where $R_0(a,r)$ and $R_2(a,r)$ are the normalized radial functions, and the dimensionless functions $u(\beta)$ and $v(\beta)$ are associated with the shape ellipticity and crystal structure, respectively [15]. When the NQD shape becomes nonspherical, the radii of circular (b) and non-circular (c) cross section can be defined as shown in Fig. 1. Compared to the radius of spherical NQD (a), prolate and oblate NQDs show $c > a > b$ and $b > a > c$ with $a = (b^2 c)^{1/3}$ respectively. Therefore, while the NQD shape changes from oblate to prolate, the degree of ellipticity ($\mu = \frac{c-b}{a}$) varies from negative to positive.

The electron-hole exchange energy E_{ex} gives rise to an additional splitting $\triangle_{ex}$ as

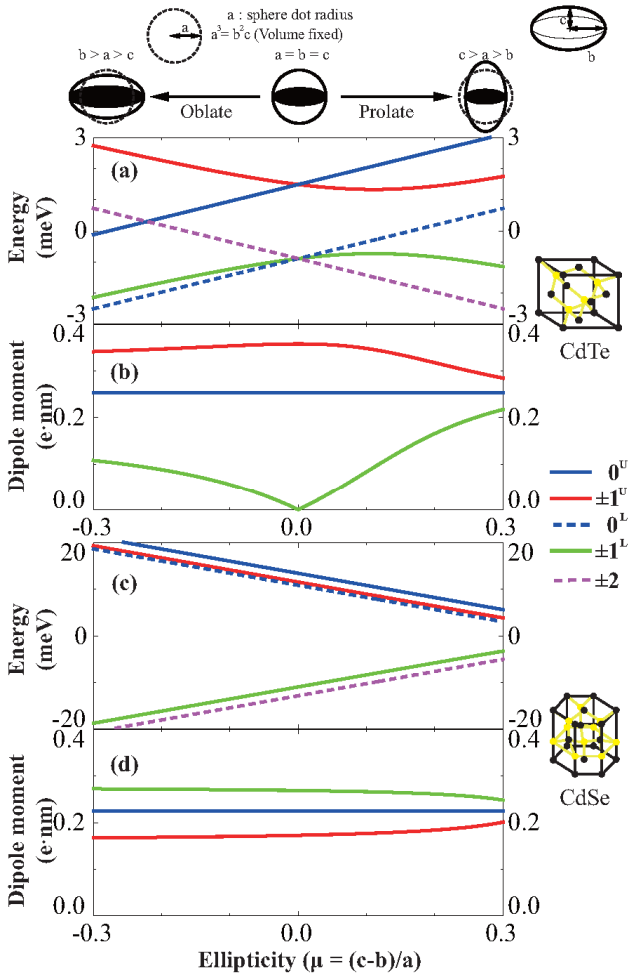

FIG. 1. Ellipticity (μ) dependence of the exciton fine energy levels (0^U, 0^L $\pm1^U$, $\pm1^L$ and, ±2) and the corresponding dipole moments in CdTe (a,b) and CdSe (c,d) QD with radius (a = 3 nm) respectively. Solid and dotted lines represent the bright exciton states ($\pm1^L$, $\pm1^U$, 0^U) and dark exciton states (0^L, ±2), respectively.

$$\triangle_{ex} = \left(\frac{a_{ex}}{a}\right)^3 E_{ex} w(\beta), \tag{4}$$

$$w(\beta) = \frac{a^2}{6}\int_0^a dr \sin^2\left(\frac{\pi r}{a}\right)\left[R_0^2(a,r) + \frac{1}{5} R_2^2(a,r) \right], \tag{5}$$

where the dimensionless function $w(\beta)$ describes the electron-hole exchange interaction, and a_{ex} is the exciton Bohr radius. Using the parameters of CdTe and CdSe summarized in Table 1 with a 3 nm-radius, the spin-degenerate five energy levels (0^U, 0^L, $\pm1^U$, $\pm1^L$ and ±2) of an exciton is given by [14]

$$E_{\pm2} = \frac{-3\triangle_{ex} - \triangle_{sh}}{2}, \tag{6}$$

TABLE 1. Parameters of CdTe and CdSe [11, 17, 18]

Properties	Constant	CdTe	CdSe
Heavy hole effective mass	m_{hh}^{*}	0.600 m_e^0	0.820 m_e^0
Light hole effective mass	m_{lh}^{*}	0.120 m_e^0	0.262 m_e^0
Electron effective mass	m_e^{*}	0.099 m_e^0	0.119 m_e^0
Energy gap	E_g	1.61 eV	1.84 eV
Crystal field energy	$\triangle_{cr}$	0 meV	25 meV
Electron-hole exchange energy	E_{ex}	0.04 meV	0.13 meV
Exciton Bohr radius	a_{ex}	7.93 nm	5.6 nm

$$E_{\pm1}^{U}=\frac{\triangle_{ex}}{2}+\sqrt{(2\triangle_{ex})^2+\left(\frac{\triangle_{sh}}{2}\right)^2-\triangle_{ex}\triangle_{sh}}\,, \tag{7}$$

$$E_{\pm1}^{L}=\frac{\triangle_{ex}}{2}+\sqrt{(2\triangle_{ex})^2+\left(\frac{\triangle_{sh}}{2}\right)^2-\triangle_{ex}\triangle_{sh}}\,, \tag{8}$$

$$E_{0}^{U}=\frac{5\triangle_{ex}+\triangle_{sh}}{2}, \tag{9}$$

$$E_{0}^{L}=\frac{-3\triangle_{ex}+\triangle_{sh}}{2}, \tag{10}$$

In order to obtain the refractive index spectrum of the exciton fine energy levels, the transition oscillator strengths of five levels were calculated as

$$\alpha_{\pm1}^{U}=\frac{1}{3}\left(1+\frac{2\triangle_{ex}-\triangle_{sh}/4}{\sqrt{(2\triangle_{ex})^2+(\triangle_{sh}/2)^2-\triangle_{ex}\triangle_{sh})}}\right), \tag{11}$$

$$\alpha_{\pm1}^{L}=\frac{1}{3}\left(1-\frac{2\triangle_{ex}-\triangle_{sh}/4}{\sqrt{(2\triangle_{ex})^2+(\triangle_{sh}/2)^2-\triangle_{ex}\triangle_{sh})}}\right), \tag{12}$$

$$\alpha_{0}^{U}=\frac{1}{3}, \tag{13}$$

where the sum of the five oscillator strength was normalized ($\alpha_{\pm1}^{U}+\alpha_{\pm1}^{L}+\alpha_{0}^{U}=1$). It is noticeable that α_0^L and $\alpha_{\pm2}$ are zero because they are optically inactive dark states [15, 16].

Given the oscillator strength (α_k) of a *k*-fine energy level (E_k), the corresponding polarization $P_k(t)$ and occupancy $f_k(t)$ can be defined and they depend on time (*t*). Additionally, the dipole moment of *k*-state can also be obtained as $d_k=e\hbar\sqrt{\frac{\alpha_k}{2M^{*}E_k}}$, where M^{*} is the total exciton effective mass, and the nonlinear refractive index can be obtained by solving the semiconductor Bloch equations (SBEs). With the electric field of a pump $(E_p(t)e^{\vec{ik}_p\cdot\vec{r}})$ and test pulse $(E_t(t)e^{\vec{ik}_t\cdot\vec{r}})$, the SBEs in an *n*-order spatial Fourier series expansion can be given as [19-21]

$$\begin{aligned}\frac{d}{dt}P_k^n(t)=&-(i\omega_{k,0}+\gamma_k)P_k^n(t)+i\Omega_{k,t}(t)(\delta_{n,1}-2f_k^{n-1}),\\&+i\Omega_{k,p}(t)(\delta_{n,-1}-2f_k^{n+1})\end{aligned} \tag{14}$$

$$\begin{aligned}\frac{d}{dt}f_k^n(t)=&\,i\left[\Omega_{k,t}(t)(P_k^{-n+1})^{*}-\Omega_{k,t}^{*}(t)P_k^{n+1}\right]\\&+i\left[\Omega_{k,p}(t)(P_k^{-n-1})^{*}-\Omega_{k,p}^{*}(t)P_k^{n-1}\right]\end{aligned}, \tag{15}$$

where the Rabi frequency of the pump and test pulse can also be defined as

$$\Omega_{k,t}(t)=\frac{d_kE_t(t)}{\hbar},\ \Omega_{k,p}(t)=\frac{d_kE_p(t)}{\hbar}, \tag{16}$$

, and the γ_k is the dephasing factor and $\hbar\omega_{k,0}$ is the fine exciton levels determined by the confinement energy and the exchange energy of electron and hole. Those equations enable us to obtain both the real ($n(\omega,\Theta)$) and imaginary ($\kappa(\omega,\Theta)$) nonlinear refractive index spectrum for an injected pump pulse area ($\Theta=\int_{-\infty}^{\infty}\Omega_{k,p}(t)dt$) [19, 22] using Fourier transformation of electric susceptibility ($\chi(\omega)=\sum_{k,n}P_k^n(\omega)/E_t(\omega)$). As the calculation considers complex number, the Kramers-Kronig relation is not necessary. It is also noticeable that high order nonlinear terms of the SBEs are sufficiently small. Thus, we calculated numerically the polarization and occupancy up to the third order (n = 3) For example, the polarization of the fifth-order effect is smaller by three-orders-of magnitude (~10^3) compared to that of the third-order effect. Therefore, the occupancy-dependent refractive index can also be described in terms of pulse area.

III. RESULTS AND DISCUSSION

Regarding ellipticity dependence of the exciton fine energy levels in CdTe (Fig. 1(a)) and CdSe (Fig. 1(c)) QDs, a significant difference was obtained. When a spherical QD of CdTe is formed, the degenerate heavy- and light-hole states become separated with $\triangle_{sh}=0$. Because the cubic

structure gives rise to $\triangle_{cr}=0$ in CdTe, the fine exciton energy levels of a spherical CdTe QD are determined only by $\triangle_{ex}$.

As shown in Fig. 1(a), the energy level difference between $\pm1^{U}$ and $\pm1^{L}$ (~2.5 meV) for a spherical CdTe QD ($\mu=0$) mainly results from the exchange interaction ($\triangle_{ex}$), which becomes increased for decreasing the confinement size ($\triangle_{ex}\sim a^{-3}$). Additionally, as the shape ellipticity becomes significant, $\triangle_{sh}$ becomes involved, i.e. $\triangle_{sh}$ becomes positive or negative for oblate and prolate structures, respectively. For a spherical CdTe QD ($\mu=0$), the dark exciton states (0^{L} and ±2) are degenerate with the same exchange interaction energy of $\triangle_{ex}$ ~1.0 meV. However, those become split as $\triangle_{sh}$ becomes significant for oblate and prolate CdTe QDs ($\mu\neq0$). As the shape ellipticity become significant, the wavefunction difference of the heavy- and light-holes states gives rise to an energy difference, which can be obtained by perturbation method. It is noticeable that the energy levels of 0^{U}, 0^{L}, and ±2 states show a monotonic dependence for μ due to the linear dependence of $\triangle_{ex}$ and $\triangle_{sh}$ (Eqs. (6), (9), and (10)), but those of $\pm1^{U}$ and $\pm1^{L}$ states for μ show a novel curve due to the nonlinear dependence of $\triangle_{ex}$ and $\triangle_{sh}$.

Shape ellipticity (μ) dependence of the fine levels is very sensitive to crystal structure, and is dominated by the non-sphericity energy ($\triangle_{sh}$). As described in Eq. (1), $\triangle_{sh}$ is associated with the crystal field energy ($\triangle_{cr}$). Regarding $\triangle_{cr}=25$ meV in CdSe and $\triangle_{cr}=0$ in CdTe, the fine level change for μ is relatively small in CdTe compared to that in CdSe. As shown in Fig. 1(c), the variation of the fine levels in CdTe is only a few meV when the ellipticity of the QD shape changes from oblate (-0.3) to prolate (0.3). On the other hand, both bright and dark levels of CdSe show a significant shift of ~20 meV for μ due to the large crystal field energy ($\triangle_{cr}=25$ meV). Therefore, the fine levels of CdSe QDs are very sensitive to shape ellipticity compared to those of CdTe QDs. Additionally, the electron-hole exchange energy of CdTe is comparable to the non-sphericity energy. Therefore, the fine level change for μ becomes nonlinear. On the other hand, the fine level change of CdSe shows a linear dependence for μ due to the relatively small electron-hole exchange energy.

In Figs. 1(a) and 1(c), both 0^{U} and 0^{L} states have the same slope $\triangle_{sh}/2$ for ellipticity (μ), and the slope of ±2 states for μ also have the same magnitude but the sign is opposite ($-\triangle_{sh}/2$). Figs. 1(b) and 1(d) show the exciton dipole moment of the fine levels in CdTe and CdSe, respectively. The dipole moments of the fine levels in CdSe barely depend on shape ellipticity. On the other hand, interesting features are seen in the dipole moment of CdTe. When CdTe forms a perfect sphere ($\mu=0$), $\pm1^{L}$ is not optically accessible with zero dipole moment. Therefore, only three bright states of 0^{U} and $\pm1^{U}$ can be observed. Interestingly, the dipole moment of 0^{U} of has no dependence on shape ellipticity both in CdTe and CdSe. The dipole moment of $\pm1^{U}$ state in CdTe (Fig. 1(b)) decreases as positive μ increases up to 0.3, and a small change of the dipole moment is seen in the $\pm1^{U}$ and $\pm1^{L}$ states of CdSe near $\mu\sim0.3$ (Fig. 1(d)). However, the dipole moment of the $\pm1^{L}$ state in CdTe (Fig. 1(b)) looks sensitive to the shape change.

In a spherical CdTe QD, the $\pm1^{L}$ state has a null dipole moment. Therefore, only the degenerate 0^{U} and $\pm1^{U}$ are optically active. When those three bright states are resonantly

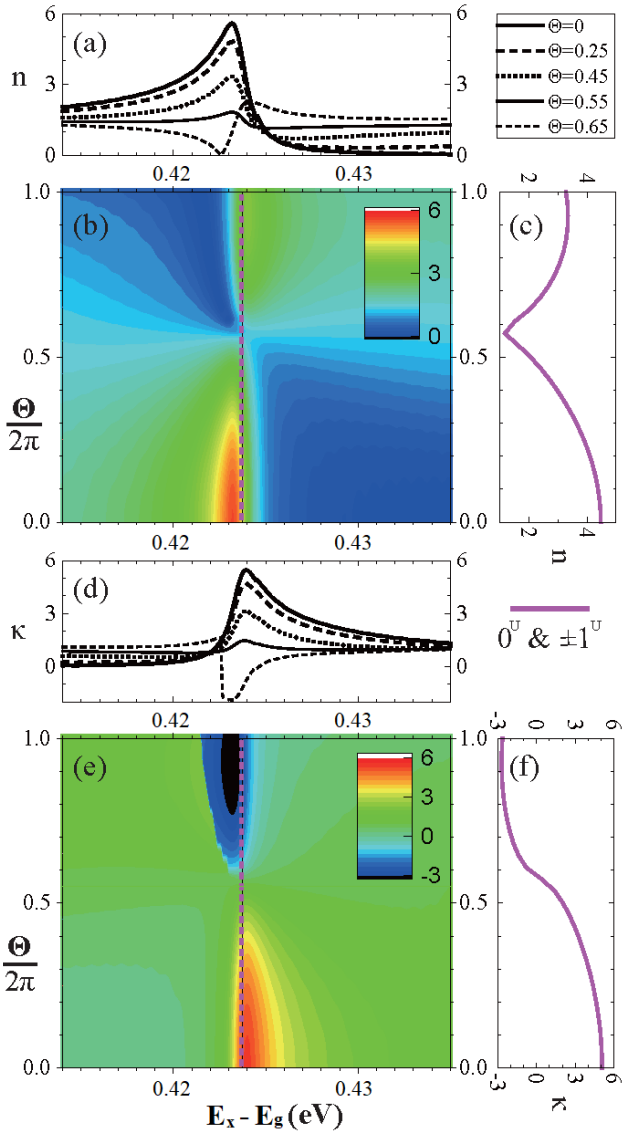

FIG. 2. Excitation dependence of the nonlinear refractive index in a spherical ($\mu=0$) CdTe quantum dot, where only the degenerate 0^{U} and $\pm1^{U}$ states are optically active and the excitation is given by 100 fs pulse area ($\Theta=\int_{-\infty}^{\infty}\Omega_{k,p}(t)dt$). For increasing Θ, the nonlinear refractive index spectrum in real (a,b,c) and imaginary parts (d,e,f) are shown. The spectral energy is given in terms of the energy difference between the lowest fine exciton levels and bulk band gap (E_X-E_g).

excited by a 100 fs laser, a change of the refractive index is induced. As shown in Figs. 2(a) and 2(b), the real part (n) of the nonlinear refractive index spectrum is shown for increasing pulse area (Θ), where the spectral energy is given in terms of the energy difference between the lowest fine exciton levels and bulk band gap ($E_X - E_g$). For the energy below the resonance level of 0^U and $\pm1^U$ states, the refractive index decreases for increasing Θ. However, the energy higher than the resonance level shows the opposite feature. As a result, the real part of the refractive index at the resonance level decreases while Θ increases up to $0.57\times2\pi$, but increases afterward (Fig. 2(c)). When this result is considered in a point of the Kerr effect, where the refractive index change shows a linear dependence for excitation intensity ($\triangle n \sim I \sim \Theta^2$), this approximation seems valid up to $\Theta \sim 0.2\times2\pi$. Likewise, the imaginary part (κ) of the nonlinear refractive index spectrum is shown for increasing pulse area (Θ) in Figs. 2(d) and 2(e). As shown in Fig. 2(f), an absorption saturation can be seen at the resonance level of 0^U and $\pm1^U$ states. When ensemble CdSe quantum dots are dispersed with a density of ~10^{12} cm^2, roughly ~80 nJ energy is necessary to give a state bleaching under resonant pulse excitation. Therefore, the full saturation can be observed near 8 μJ of pulse excitation when single quantum dot is excited by a pico-second pulse.

While a single degenerate bright level consists of three bright states of 0^U and $\pm1^U$ in CdTe QDs, three separate bright levels are given in CdSe QDs, where 0^U, $\pm1^U$, and $\pm1^L$ are located in the highest, intermediate, and lowest levels, respectively. Because those states have similar dipole moments, nonlinear modulation of a laser pulse depends on spectral tuning. We calculated the central energy of our laser near the resonance energy of $\pm1^L$ which has a spectral width of ~20 meV. Therefore, the nonlinearity is dominated by $\pm1^L$ states, but the contribution of $\pm1^U$ and 0^U states are not negligible as shown in Fig. 3(a). As excitation dependence of the real refractive index spectrum is shown as a contour map in Fig. 3(b), a refractive index change at a certain spectral energy can also be plotted as shown in Fig. 3(c). It is noticeable that the refractive index change of $\pm1^L$ states becomes maximized when $\Theta \sim \pi$, but other high levels need stronger excitation to obtain a similar change.

Likewise, excitation dependence of the imaginary part were also shown in Figs. 3(d), 3(e), and 3(f). When $\Theta \geq \pi$, extinction coefficient (κ) near $\pm1^L$ states becomes negative, i.e. gain. However, other states of $\pm1^U$ and 0^U are not saturated with $\Theta \sim \pi$. When excitation is weak enough ($\Theta \lesssim 0.2\times2\pi$), those optical nonlinearities of $\triangle n$ and $\triangle\kappa$ can also be approximated into the Kerr effect ($\sim\Theta^2$). The slope of refractive index change for excitation can be decreased while the pulse duration becomes elongated from femtosecond to picosecond. For intuitive understanding, it is noticeable that this model is based on semi-classical light-matter interaction. While the excitation intensity is

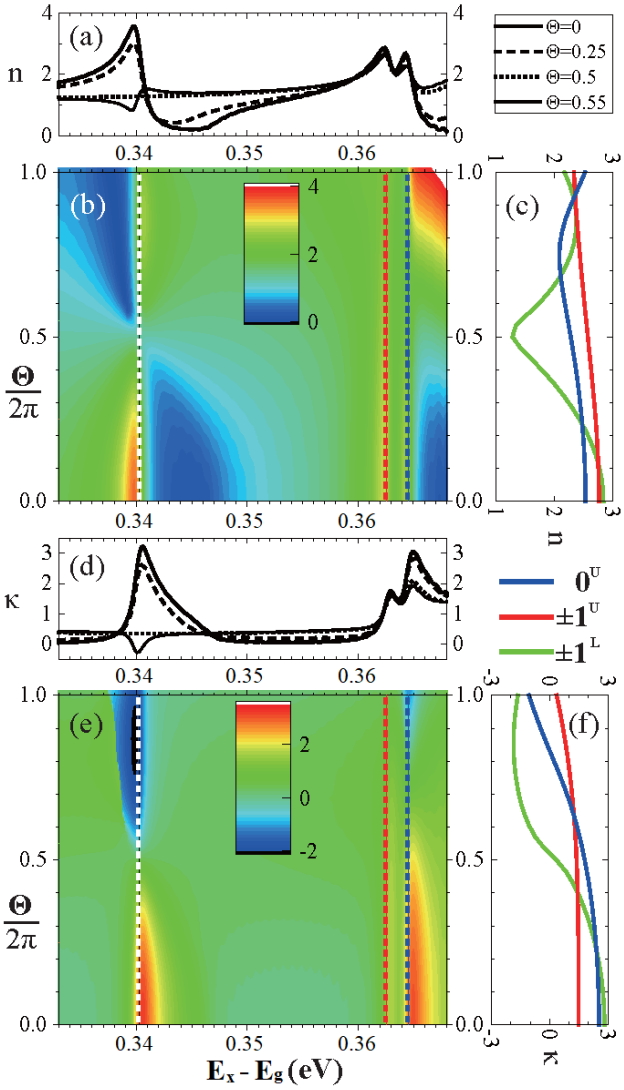

FIG. 3. Excitation dependence of the nonlinear refractive index in a spherical ($\mu=0$) CdSe quantum dot, where $\pm1^L$, 0^U, and $\pm1^U$ states are optically active and the excitation is given by 100 fs pulse area (Θ). For increasing Θ, the nonlinear refractive index spectrum in real (a,b,c) and imaginary parts (d,e,f) are shown.

similar to classical nonlinear optics, the state filling plays an important role. Therefore, the state occupancy (f) gives rise to a unique feature compared to the classical nonlinear optics.

As shown in Fig. 4(a), the occupancy of the bright states in a spherical CdTe increases as pulse area (Θ) is increased up to π. However, for $\Theta > \pi$, the occupancy decreases gradually. This result implies a transient stimulated emission, where the negative extinction coefficient ($\kappa < 0$) is seen in Fig. 2(d). It is noticeable that the occupancy of 0^U becomes saturated when $\Theta \sim 0.7\times2\pi$, and this can be explained by the relatively small oscillator strength. The occupancy of $\pm1^L$ remains zero as it is an optically forbidden dark state.

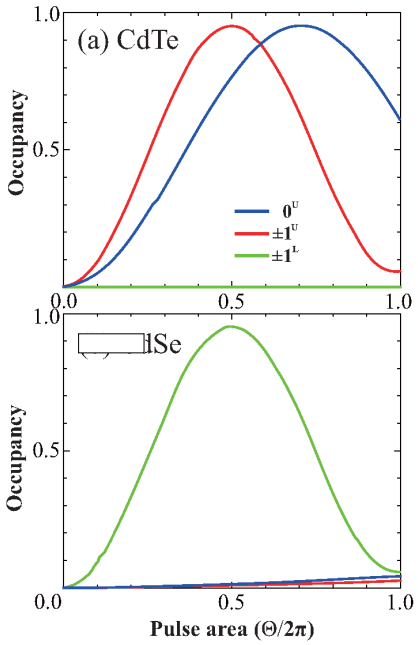

FIG. 4. With increasing excitation pulse area, the occupancy of the bright (0^U and $\pm1^U$) states are shown in a spherical CdTe (a) and CdSe (b) quantum dot, respectively. Notice that the central laser energy are tuned at the lowest bright state and dephasing effect is ignored.

Figure 4(b) shows the occupancy of the bright states in a spherical CdSe for increasing pulse area (Θ). While only one energy level is involved in a spherical CdTe quantum dot, three different energy levels are involved in a spherical CdSe quantum dot. We found that the occupancy of the lowest bright level ($\pm1^L$) becomes saturated when $\Theta \sim \pi$, but the other two levels (0^U and $\pm1^U$) show small occupancy (<0.1). Therefore, one may assume that optical nonlinearities of a spherical CdSe quantum dot are dominated by $\pm1^L$.

In Fig. 5, we also considered shape dependent optical nonlinearities. With increasing excitation pulse area (Θ), the normalized real ($\Delta n(\Theta)/n(\Theta=0)$) and imaginary ($\Delta\kappa(\Theta)/\kappa(\Theta=0)$) refractive index change at the bright states of $\pm1^L$, $\pm1^U$ and, 0^U were plotted, where three different shapes, oblate ($\mu=0.1$) (Figs. 5(a) and 5(d)), sphere ($\mu=0$) (Figs. 5(b) and 5(e)), and prolate ($\mu=0.1$) (Figs. 5(c) and 5(f)), were compared in CdTe and CdSe, respectively. For the resonant energy levels of the bright exciton states ($\pm1^L$, $\pm1^U$ and, 0^U), we considered the shape dependent energy levels in CdTe (Fig. 1(a)) and CdSe (Fig. 1(c)).

In the case of oblate shape QDs, both CdTe and CdSe QDs show a similar feature of optical nonlinearities up to $\Theta \sim \pi$. However, for $\Theta \sim \pi$, the imaginary part change in

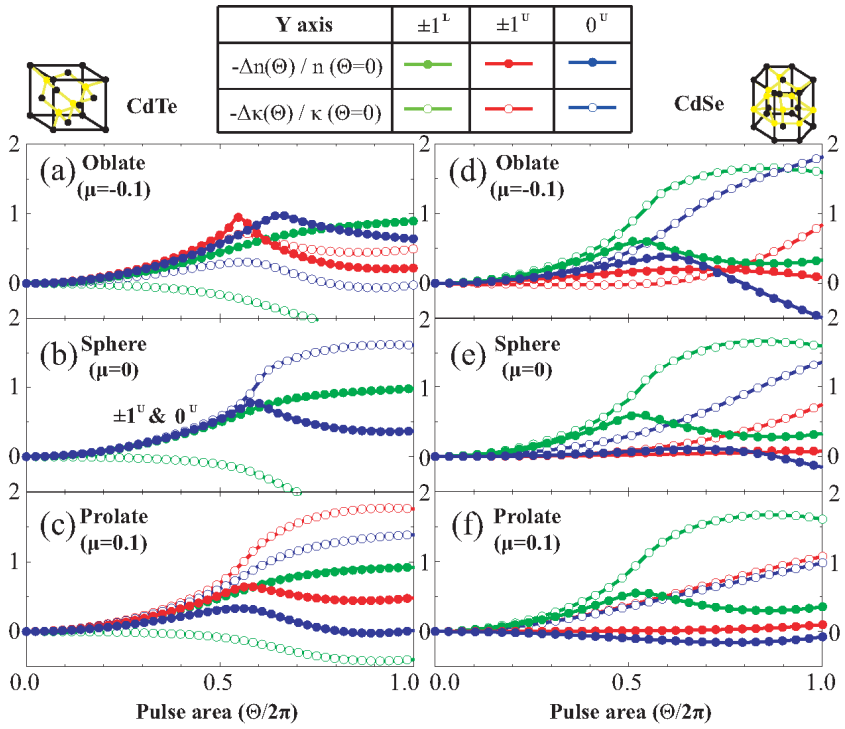

FIG. 5. Refractive index of the bright states ($\pm1^L$, $\pm1^U$ and, 0^U) vary with increasing excitation pulse area (Θ), where the real ($\Delta n = n(\Theta \geq 0) - n(\Theta = 0)$) and imaginary ($\Delta\kappa = \kappa(\Theta \geq 0) - \kappa(\Theta = 0)$) refractive index change for Θ are normalized by the linear real ($n(\Theta = 0)$) and imaginary ($\kappa(\Theta = 0)$) refractive index without excitation, respectively. Shape-dependent optical nonlinearities of the bright states in CdSe and CdTe are shown in terms of the normalized refractive index change in real ($\Delta n(\Theta)/n(\Theta = 0)$) and imaginary ($\Delta\kappa(\Theta)/\kappa(\Theta = 0)$) parts. With the same oblate (a,d), sphere (b,e), prolate (c,f) structures, a different optical nonlinearity is significant between CdTe and CdSe quantum dots due to the crystal structure difference.

CdSe QDs becomes dominant compared to those in CdTe QDs. In the case of spherical ($\mu = 0$) QDs, one may easily understand how Figs. 5(b) and 5(e) can be obtained from Figs. 2 and 3. In spherical CdTe QDs, it is noticeable that the real refractive index change of the five bright states ($\pm 1^{L}$, $\pm 1^{U}$ and, 0^{U}) increases with the same manner up to $\Theta \sim \pi$, and this looks suitable for phase modulation. Prolate CdTe QDs ($\mu = 0.1$) are also useful for phase modulation as the real and imaginary refractive index change show a similar feature up to $\Theta \sim \pi$ (Fig. 5(c)).

IV. CONCLUSION

We found that the crystal structure difference of CdTe (cubic) and CdSe (wurtzite) gives a significant difference in linear and nonlinear optical properties although the same radii of spherical quantum dots are given. Additionally, shape ellipticity dependence of the dipole moment was considered for the exciton fine levels. For increasing excitation pulse area, the nonlinear refractive index of the fine exciton levels were also obtained using the semiconductor Bloch equations.

REFERENCES

1. A. I. Ekimov, Al. L. Efros, and A. A. Onushchenko, "Quantum size effect in semiconductor microcrystals," Solid State Commun. **56**, 921-924 (1985).
2. Z.-W. Wang, W.-P. Li, J.-W. Yin, and J.-L. Xiao, "Properties of parabolic linear bound potential and coulomb bound potential quantum dot qubit," Commun. Theor. Phys. **49**, 311-314 (2008).
3. F. Pinaud, X. Michalet, L. A. Bentolila, J. M. Tsay, S. Doose, J. J. Li, G. Lyer, and S. Weiss, "Advances in fluorescence imaging with quantum dot bio-probes," Biomaterials **27**, 1679-1687 (2006).
4. A. I. Ekimov, F. Hache, M. C. Schanne-Klein, D. Ricard, C. Flytzanis, I. A. Kudryavtsev, T. V. Yazeva, A. V. Rodina, and Al. L. Efros, "Absorption and intensity-dependent photoluminescence measurements on CdSe quantum dots: assignment of the first electronic transitions," J. Opt. Soc. Am. B **10**, 100-107 (1993).
5. B. De Geyter and Z. Hens, "The absorption coefficient of PbSe/CdSe core/shell colloidal quantum dots," Appl. Phys. Lett. **97**, 161908 (2010).
6. A. Gaur, B. D. Shrivastava, and H. L. Nigam, "X-Ray absorption fine structure (XAFS) spectroscopy - A review," Proc. Indian. Natn. Sci. Acad. **79**, 921-966 (2013).
7. H. Ping, "Effect of dielectric constant on the exciton ground state energy of CdSe quantum dots," Chin. Phys. **9**, 844-847 (2000).
8. S. W. Koch, N. Peyghambarian, and M. Lindberg, "Transient and steady-state optical nonlinearities in semiconductors," J. Phys. C: Solid State Phys. **21**, 5229-5249 (1988).
9. Al. L. Efros, "Luminescence polarization of CdSe microcrystals," Phys. Rev. B **46**, 7448-7458 (1991).
10. Al. L. Efros and A. V. Rodina, "Band-edge absorption and luminescence of nonspherical nanometer-size crystals," Phys. Rev. B **47**, 10005-10007 (1996).
11. Al. L. Efros, M. Rosen, M. Kuno, M. Nirmal, D. J. Norris, and M. Bawendi, "Band-edge exciton in quantum dots of semiconductors with a degenerate valence band: Dark and bright exciton states," Phys. Rev. B. **54**, 4843-4856 (1996).
12. V. I. Klimov, *Nanocrystal quantum dots* (CRC Press, 2010).
13. D. J. Norris and M. G. Bawendi, "Measurement and assignment of the size-dependent optical spectrum in CdSe quantum dots," Phys. Rev. B. **53**, 16338-16346 (1995).
14. E. O. Kane, "Band structure of indium antimonide," J. Phys. Chem. Solids **1**, 249-261 (1957).
15. C. R. Pidgeon and R. N. Brown, "Interband magneto-absorption and faraday rotation in InSb," Phys. Rev. **146**, 575-583 (1966).
16. M. Nirmal, D. J. Norris, M. Kuno, M. G. Bawendi, Al. L. Efros, and M. Rosen, "Observation of the "Dark exciton" in CdSe quantum dots," Phys. Rev. Lett. **75**, 3728-3731 (1995).
17. A. Rubio-Ponce, D. Olguin, and I. Hernandez-Calderon, "Calculation of the effective masses of 2-6 semiconductor compounds," Superficies Vacio **16**, 26-28 (2003).
18. G. Fonthal, L. Tirado-Mejia, J. I. Marin-Hurtado, H. Ariza-Calderon, and J. G. Mendoza-Alvarez, "Temperature dependence of the band gap energy of crystalline CdTe," J. Phys. Chem. Solids **61**, 579-583 (2000).
19. M. Lindberg, R. Binder, and S. W. Koch, "Theory of the semiconductor photon echo," Phys. Rev. A **45**, 1865-1875 (1992).
20. H. Haug and S. W. Koch, *Quantum theory of the optical and electronic properties of semiconductors* (World Scientific, 1990).
21. N. Van Trong and G. Mahler, "Field-dependent screening and dephasing in semiconductor Bloch equations," Phys. Rev. B **54**, 1766-1774 (1996).
22. K.-C. Je, I.-C. Shin, J. Kim, and K. Kyhm, "Optical nonlinearities of fine exciton states in a CdSe quantum dot," Appl. Phys. Lett. **97**, 103110 (2010).